International Journal of Engineering and Technology Innovation, vol. 5, no. 2, 2015, pp. 87-98

Numerical Investigation of Film Cooling from Two Rows of Holes with Anti-Vortex Holes Attached to the Upstream Row

Mostafa Abdelmohimen Hussien Abdelmohimen*

Department of Mechanical Engineering, Shoubra Faculty of Engineering, Benha University, Egypt

Received 14 June 2014; received in revised form 04 December 2014; accepted 02 February 2015

Abstract

Computational analysis of film cooling effectiveness from two rows of holes inclined with 30^o on a flat surface in case of in-line and staggered arrangements has been carried out. The upstream row is supplemented with anti-vortex holes. The addition of anti-vortex holes is presented as a new technique depends on adding two cylindrical holes branching out from the main holes. Three different positions of anti-vortex holes are studied with three different values of velocity ratios. The study is carried out using realizable *k-ϵ model* in FLUENT commercial code. The numerical model is verified by comparing a single row of film cooling holes results with available experimental works in literature. The results ensure that the staggered arrangement gives higher film cooling effectiveness than the in-line one for all studied velocity ratios. The use of anti-vortex holes increases the film cooling effectiveness. The position of anti-vortex holes shows a significant effect, especially with high velocity ratios.

Keywords: Film Cooling; Two rows; Anti-Vortex; CFD

1. Introduction

The film cooling effectiveness characteristics with lateral injection was described by Goldstein et al. [1]. Two inclination angles of 15 and 35 deg. were investigated. Andreopoulous and Rodi [2] studied the interaction behavior of a single jet and mainstream. The jet is pushed towards the bottom wall and the mainstream is deflected as if the jet forms a solid boundary. Formation of kidney vortices appears as a result of the interaction, i.e. a pair of counter rotating vortices as described by Haven et al. [3]. There are two undesirable effects due to these vortices. The First one is that, the hot mainstream air is forced to move down the jet, thus heating the turbine blade wall. The second one is that, the mutual interaction between the vortex pair tends to lift the jet off the turbine blade surface which reduces the film cooling. Lemmon et al. [4] showed that these vortices are caused by the bending of the jet by the mainstream and not by viscous wall effects in the hole or plenum.

Alok Dhungel [5] investigated the film cooling enhancement due to the use of anti-vortex holes. Both heat transfer coefficient and film cooling effectiveness are determined experimentally. A total of six different cases with variations in geometry and orientation of the anti-vortex holes in relation to the main film cooling holes are investigated. The Results showed that the presence of anti-vortex holes mitigates the effect of the pair of anti-vortices. Heidmann [6] and Heidmann et al. [7] studied numerically the effect of adding the anti-vortex holes. They used a 3–D Navier-Stokes solver Glenn-HT which has been conceived and developed at NASA Glenn Research Center. Mostafa et al. [8] studied numerically and experimentally the effect

* Corresponding author. E-mail address: mostafa.abdelmohimen@feng.bu.edu.eg
Tel.: +966-56-0383210

of adding anti-vortex holes on the film cooling effectiveness at different velocity ratios. Four different cases were studied. They show that there are two vortices coming out from the anti-vortex holes and working against the vortices coming out from the main hole. These vortices try to damp the main hole flow and keep it near the surface.

Film cooling performance from cylindrical cooling holes can be increased by arranging them in double rows, with the holes either in-lined or staggered [9, 10]. The presence of the upstream row of holes discourages the downstream row from lifting off the surface, thus increasing the effectiveness of this row. When the holes are arranged in staggered rather than in-line rows, the spanwise uniformity of effectiveness and heat transfer coefficient is improved. Ligrani et al. [11] investigated that in the film cooling from two rows of holes, the compound angle injection provides significantly improved protection compared to simple angle configuration.

The rows of film cooling holes are arranged in groups of closely spaced holes. In common practice there are as few as one and as many as five rows in a group (Muska et al. [11]). There are large differences in film cooling performance between staggered and in-line configurations may be considered. Afejuku et al. [12] shows that the staggered configuration showed better performance than the in-line configuration for the simple angle injection.

Jubran and Maiteh [13] studied experimentally the film cooling and heat transfer from a combination of two rows of simple and/or compound angle holes in in-line and/or staggered configuration. Their results showed the using combination of one row of downstream compound angle holes with another upstream simple injection holes row provides a significant injections holes or compound angle holes. Joon Ahn et al. [14] represent the Film cooling from two rows of holes with opposite orientation angles. They measured the boundary layer temperature distributions in the streamwise normal plane to illustrate the interaction between the injectant from the holes in the upstream row and from the downstream row. Detailed adiabatic film cooling effectiveness distributions were also measured by using thermochromics liquid crystal to investigate how well the injectant covers the film cooled surface. They showed that when the blowing ratio exceeds unity the injectant tends to lift off from the wall due to the increase of the wall normal momentum. With the in-line configuration, not like other configurations, the injectant is still well attached to the wall with the help of the downwash flow formed at the hole exit.

A computational study of film cooling from single and two staggered rows of novel semi-circular cooling holes including coolant plenum was carried out by Asghar and Hyder [15]. In their work, velocity profiles from the separate coolant plenum geometry are used for inlet condition to cooling holes. Realizable k-ϵ turbulence model with enhanced wall treatment is used for turbulence modeling in simulations. It is observed that coolant jet heights for one row and two staggered rows of semi-circular holes are lower than that for one row of circular holes. The centerline and laterally averaged effectiveness values from a row of semi-circular holes are found almost same as that from a row of circular holes due to the less jet lift-off in semi-circular case. Semi-circular hole utilizes half of the coolant mass required for full circular hole for producing the same blowing ratio, so same level of effectiveness from semi-circular holes as that from full circular holes is great advantage.

The present paper aims at investigating numerically the film cooling from two rows of holes the upstream one is supplemented with anti-vortex holes. This technique which is used with single row of holes is promising to give more enhancements in film cooling from two rows of holes.

2. Numerical technique

The studied cases geometries are generated by the GAMBIT pre-processor. Triangle Pave mesh, which was used to generate the grids, produces grids with unstructured, smooth, and T- grid hybrid elements throughout the volumetric region.

Around 1.6 million computational cells were used for each case. The study is carried out using realizable k-ε model in FLUENT commercial code. The residual levels are about 10^{-7} for velocity components and energy equation and 10^{-5} for mass flow rate. An investigation of grid independence was carried out to find the proper mesh.

2.1. Governing equations in turbulence model

The governing equations to be solved are the incompressible continuity, momentum, and energy equations and the transport equations for the turbulent kinetic energy, and dissipation added through the turbulence models. The fluid properties are assumed constant, which is a reasonable assumption compared to the corresponding experiments.

$$\frac{\partial U_i}{\partial x_i} = 0 \tag{1}$$

$$\frac{\partial U_i}{\partial t} + \frac{\partial (U_j U_i)}{\partial x_j} = -\frac{1}{\rho}\frac{\partial P}{\partial x_i} + \frac{\partial}{\partial x_j}(2\nu S_{ij} - \overline{u_i' u_j'}) \tag{2}$$

$$\frac{\partial T}{\partial t} + \frac{\partial (U_j T)}{\partial x_j} = \frac{\partial}{\partial x_j}(\frac{\nu}{Pr}\frac{\partial T}{\partial x_j} - C_p\overline{T' u_j'}) \tag{3}$$

Equations (1) and (2) are called Reynolds-averaged Navier-Stokes (RANS) equations. Where Sij is the mean rate of strain tensor, $\tau_{ij} = -\overline{u_i' u_j'}$ is known as the specific Reynolds stress tensor, and $C_p\overline{T' u_j'}$ represents the specific turbulent heat flux. Both of these two terms need to be modeled. The present work employs the Realizable $k-\epsilon$ model for simulation of turbulent flow in film cooling and the velocity vector plots.

The modeled transport equations for k and ϵ in the realizable k- ϵ model (Shih et al. [16]) are

$$\frac{\partial}{\partial t}(\rho k) + \frac{\partial}{\partial x_i}(\rho k u_j) = \frac{\partial}{\partial x_i}\left[\left(\mu + \frac{\mu_t}{\sigma_k}\right)\frac{\partial k}{\partial x_j}\right] + G_k + G_b - \rho\epsilon - Y_M + S_k \tag{4}$$

$$\frac{\partial}{\partial t}(\rho \epsilon) + \frac{\partial}{\partial x_j}(\rho \epsilon u_j) = \frac{\partial}{\partial x_j}\left[\left(\mu + \frac{\mu_t}{\sigma_\epsilon}\right)\frac{\partial \epsilon}{\partial x_j}\right] + \rho C_1 S_\epsilon - \rho C_2 \frac{\epsilon^2}{k + \sqrt{v\epsilon}} + C_{1\epsilon}\frac{\epsilon}{k}C_{3\epsilon}G_b + S_\epsilon \tag{5}$$

Where $C_1 = max\left[0.43, \frac{\eta_1}{\eta_1 + 5}\right]$ (6)

and $\eta_1 = S\frac{k}{\epsilon}$

In the above equations, G_k represents the generation of turbulence kinetic energy due to the mean velocity gradients, and may be defined as

$$G_k = -\rho\overline{u_i' u_j'}\frac{\partial u_j}{\partial x_i} \tag{7}$$

G_b is the generation of turbulence kinetic energy due to buoyancy, and may be given by

$$G_b = \beta g_i \frac{\mu_t}{Pr_t}\frac{\partial T}{\partial x_i} \tag{8}$$

Where Pr_t is the turbulent Prandtl number for energy and g_i is the component of the gravitational vector in the ith direction. The default value of Pr_t is 0.85.

Y_M represents the contribution of the fluctuating dilatation in compressible turbulence to the overall dissipation rate, and it may be given by

$$Y_M = 2\rho\epsilon M_t^2 \tag{9}$$

Where M_t is the turbulent Mach number, defined as

$$M_t = \sqrt{\frac{k}{a^2}}$$

Where a ($\equiv \sqrt{\gamma RT}$) is the speed of sound.

2.2. *Geometry and grid details*

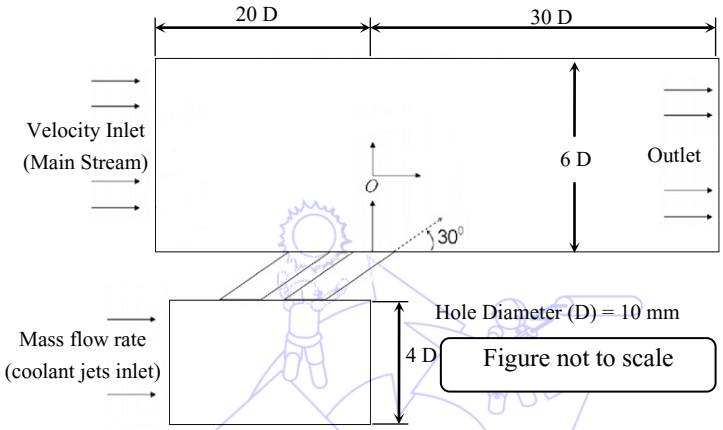

Fig. 1 Cross sectional view (as seen from z-direction) of the geometrical model

A cross-sectional view (as seen from z-direction) of the geometrical model is shown in Fig.1 Eight different models with two rows of cylindrical holes are studied. The film cooling holes are provided with a pair of anti-vortex holes to the upstream row in six models. Each model has a different anti-vortex hole geometry and orientation. Each row in in-line arrangement has a total of five film cooling holes, while in staggered arrangement the upstream raw has four holes.

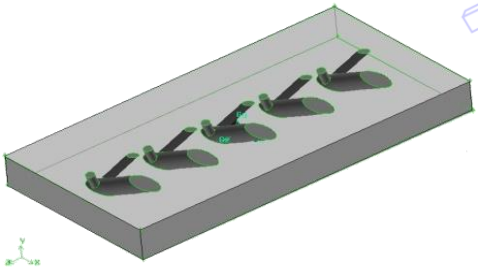

Fig. 2 Upstream Row with Anti-Vortex Holes

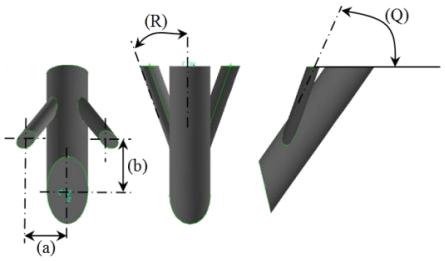

Fig.3 Anti-Vortex Hole Configuration

The total number of holes is taken in consideration when the mass flow rate through coolant jets is calculated to get the required velocity ratio through each hole. The diameter of each primary hole is 10 mm and the spacing between the holes is 3D. The length of holes is 4D. All holes are inclined to the horizontal at an angle of 30 deg. along the flow direction. A pair of anti-vortex holes are added each to all the film cooling holes in the upstream row in six cases. Fig. 2 shows an upstream row with anti-vortex holes. The diameter of each anti-vortex hole is 5 mm, (i.e. half of the primary hole diameter). The details of the anti-vortex geometry are presented in Fig. 3 Parameter 'a' is used to represent the distance between the center of the anti-vortex holes and the center of the primary film cooling holes measured in the x- direction. The similar distance measured in the y-direction is given by parameter 'b'. Parameter 'R' is used to represent the angle measured in degrees between the axis of the primary film cooling holes and the anti-vortex holes measured in the front vertical. Similar angle measured in the side vertical

plane is represented by parameter 'Q'. Parameters 'D' and 'd' represent the diameters of the primary film cooling holes and the anti-vortex holes respectively [8]. The values of all parameters for studied configurations are shown in Table 1.

Table 1: Anti-vortex holes details (related to Fig. 3)
(Dimensions in mm and angles in degrees)

	Configuration- 1	Configuration-2	Configuration-3
D	10	10	10
d	5	5	5
a	10	10	10
b	30	15	0
Q	90	49.1	30
R	30	30	30

Configuration-1 (Far-upstream anti-vortex holes) (Fig. 4 (a)): In this configuration, the anti-vortex holes shoot out vertically upwards from the primary film cooling holes. The exit of the anti-vortex holes is far upstream as compared to the exit of the primary film cooling holes. The anti-vortex holes branch out from the lower end of the primary film cooling holes.

Configuration-2 (upstream anti-vortex holes) (Fig. 4 (b)): In this configuration, the exit of the anti-vortex film cooling holes are still upstream to the outlet of the primary film cooling hole but isn't far as compared to configuration-1.

Configuration-3 (In-line Anti-vortex holes) (Fig. 4 (c)): In this configuration, the exit of the anti-vortex film cooling hole geometry is in-line with the primary film cooling holes. The anti-vortex holes branch out near the middle point of the primary film cooling holes.

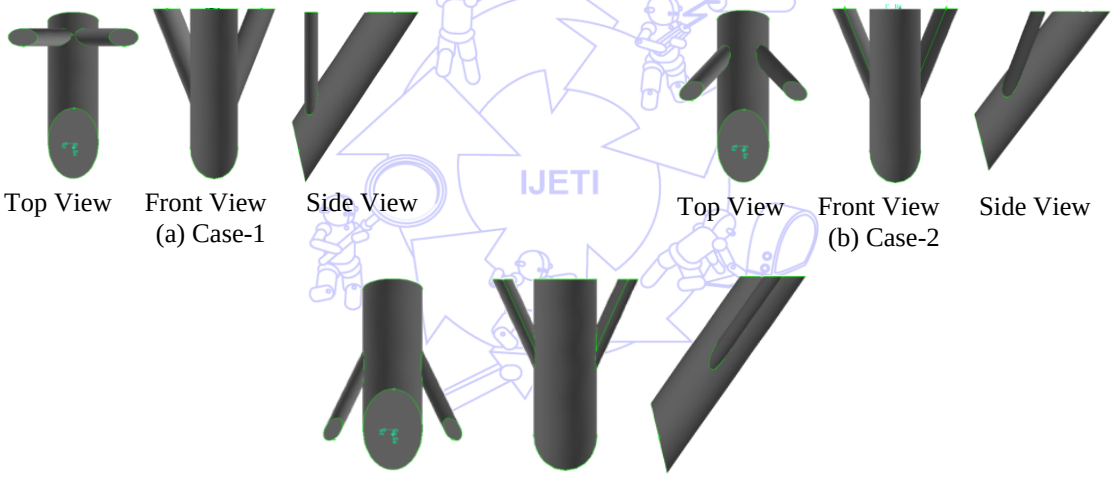

Fig. 4 Anti-Vortex Hole Orientation

The studied models specifications are simplified and presented in Table 2. Fig. 5 shows top view of test plate (as seen from y-direction) for different models studied. The grid quality near the film cooling holes is shown in Fig. 6.

Table 2: Injection models specifications

Model	Upstream row / Downstream row	Rows Arrangement
SSI	Simple / Simple	In-line
SSS	Simple / Simple	Staggered
ASI1	Anti-Case1 / Simple	In-line
ASS1	Anti-Case1 / Simple	Staggered
ASI2	Anti-Case2 / Simple	In-line
ASS2	Anti-Case2 / Simple	Staggered
ASI3	Anti-Case3 / Simple	In-line
ASS3	Anti-Case3 / Simple	Staggered

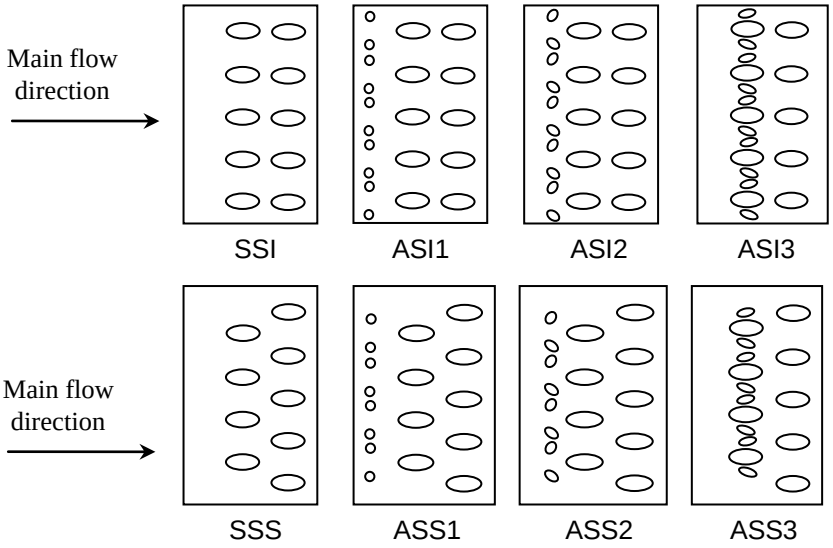

Fig. 5 Top view of test plates from +y-direction for all studied models

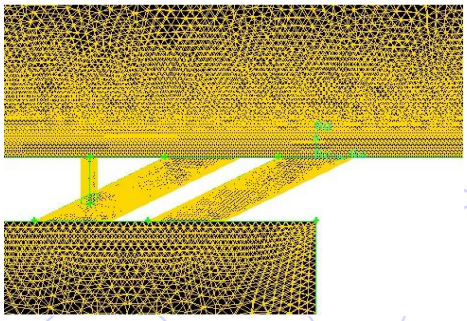

Fig. 6 grid quality near the film cooling holes for case ASI1

2.3. *Boundary conditions*

Walls boundary condition is taken as adiabatic wall boundary condition with no-slip boundary condition. It is set as: $U_w = 0, V_w = 0, W_w = 0, \overline{u_i' u_j'} = 0$ where index w denotes the wall at all boundaries except those denoted as "main stream", "coolant jets inlet", and outlet in Fig. 1. Mainstream conditions are maintained the same in all cases as (velocity – inlet) (mainstream velocity 10 m/s, and temperature 333k). The plenum inlet mass flow rate was adjusted to produce the desired velocity ratio. Table 3 shows the free-stream Reynolds number, injectant Reynolds numbers, blowing ratios, and momentum ratios related to the studied velocity ratios. The mainstream inlet total temperature was set to 2 times the plenum inlet total temperature. Turbulence intensity of 1 percent and a turbulence length scale of 1D were specified at both the mainstream inlet and plenum inlet. The following equation is used to calculate the film cooling effectiveness [7, 17, and18].

$$\eta = \frac{T_m - T_{aw}}{T_m - T_c} \tag{10}$$

Table 3: Values of Reynolds numbers, blowing ratios, and momentum ratios related to the studied velocity ratios

VR	0.5	1	2
Re_x	105065	105065	105065
Re_D	3095	6190	12380
BR	0.547	1.095	2.189
MR	0.274	1.095	4.38

3. Results and discussion

3.1. Comparison with previous studies

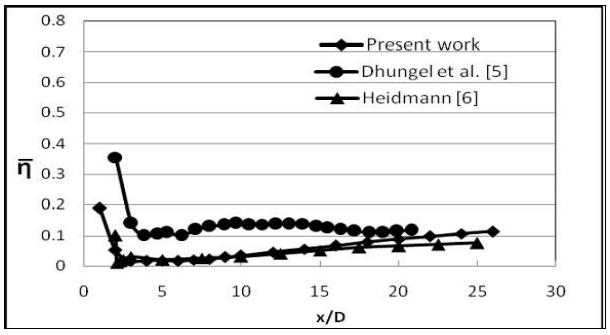

Fig. 7 Spanwise-Averaged film cooling effectiveness of single row of circular holes at VR = 2.

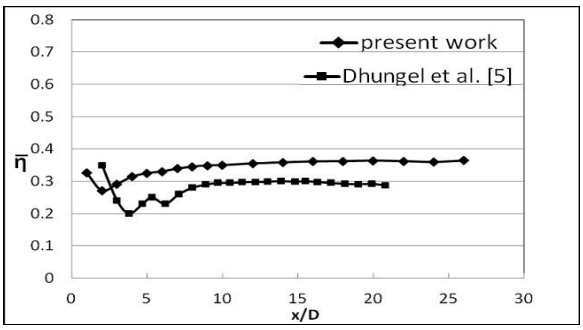

Fig. 8 Spanwise-Averaged film cooling effectiveness of single row of holes supplemented by far upstream anti-cortex holes (Case-1) at VR = 2.

For validation purpose of CFD model, present computational results of Span-wise averaged film cooling effectiveness are compared with the previous experimental results available in literature. The present CFD model was applied for a single row of film cooling holes inclined by 30o at VR = 2 and compared with the experimental results of Dhungel et al. [5] and numerical results of Heidmann, J. D [6]. The CFD model was applied also for a single row supplemented with anti-vortex holes following the first technique that is used in this research (Case-1). Dhungel et al. [5] results was taken for 0.5 inch main hole diameter with angle of inclination equal to 30o. They used infrared camera to measure the temperature distribution on the test surface. The results of Heidmann were carried out by using the 3–D Navier-Stokes solver Glenn-HT. Fig. 7 and 8 show a comparison between the using of the present work CFD model and the results of Dhungel and Heidmann for single row of holes and single row of holes supplemented by anti-vortex holes respectively. Fig. 9 shows results of the present work of model SSS as compared with Jubran and Maiteh [13] at VR = 0.5. They used Copper-Constantan thermocouples in measurements. Their holes diameter was 13 mm and inclined at 35o with respect to the test surface.

It can be seen that the computational results have the same trend as compared with the previous experimental results. On the other hand, the computational predictions in some cases are higher than that the experimental data. It has always been indicated by the previous film cooling prediction studies that the CFD results cannot predict the spreading of jets accurately.

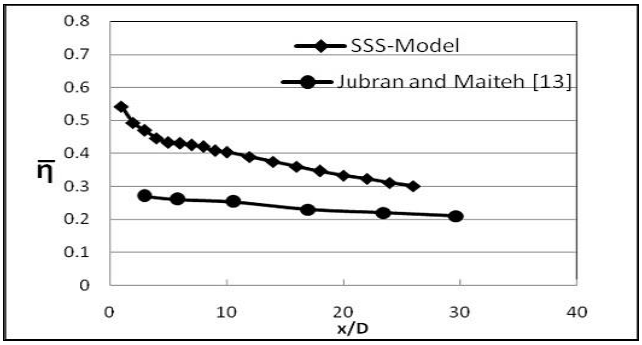

Fig. 9 Spanwise-Averaged film cooling effectiveness of SSS model at VR = 2.

3.2. Spanwise-averaged film cooling effectiveness

The spanwise-averaged film cooling effectiveness was calculated for points from z/D = 1.5 to z/D = -1.5, it means that the span averaged film cooling effectiveness will be presented downstream the middle hole. Figs. 10 and 11 show the spanwise-averaged film cooling effectiveness of different models for in-line and staggered arranges respectively at different velocity ratios. Fig. 10 shows that the lowest effectiveness along the test surface is given by model SSI for all studied velocity ratios. As the anti-vortex holes are added the film cooling effectiveness increases. At VR = 0.5, the film cooling effectiveness begins with high value near the film cooling holes exit and decreases gradually as x/D increases for all studied models. This is

due to the low momentum and mass flow rate of the cooling jets which gives it no ability to penetrate the main-stream flow and moving beside the surface. As the velocity ratio increases the momentum of the cooling jets increases and cooling jets will have the ability to penetrate the main-stream flow. At VR = 2, for model SSI the film cooling effectiveness starts with high value at the jets holes outlet and decreases suddenly downstream the jets holes due to high momentum of the film cooling jets. At x/D = 5 the film cooling effectiveness begins to increase again due to the mixing between the hot and the cold streams. By adding the anti-vortex holes, the film cooling effectiveness increases along the test surface. Models ASI1 and ASI2 give the same profile as compared with SSI model, while with model ASI3, the film cooling effectiveness starts from high value and decreases gradually along the test surface. This is due to the outlet flow of the anti-vortex holes is moving beside the outlet flow of the upstream main holes.

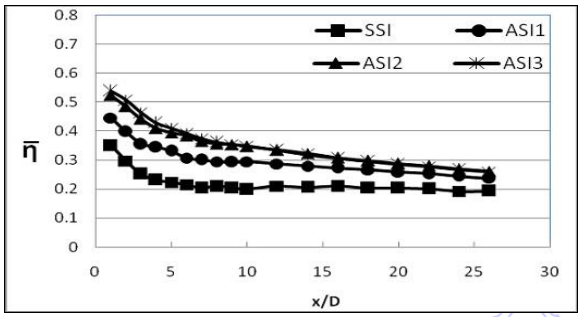

(a)VR = 0.5

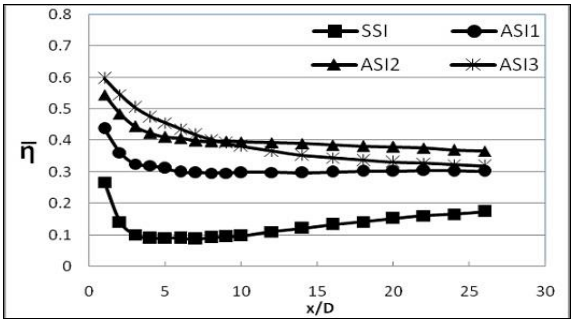

(b)VR = 1.0

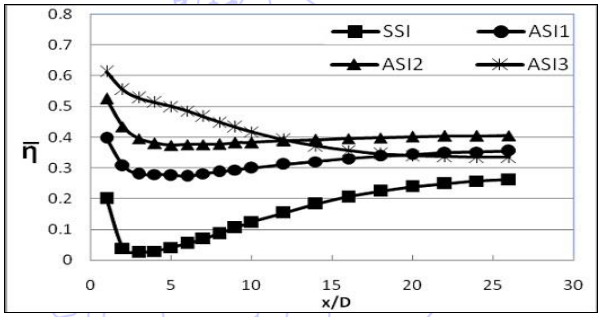

(c)VR = 2.0

Fig. 10 Spanwise-Averaged film cooling effectiveness of different models for in-line arrangement

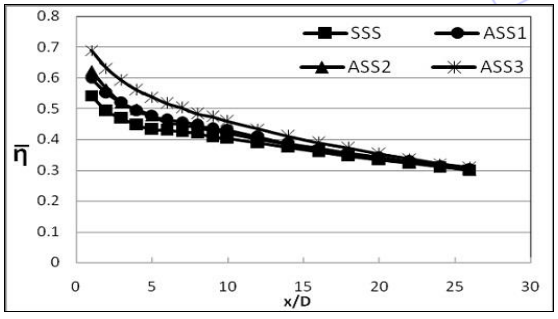

(a)VR = 0.5

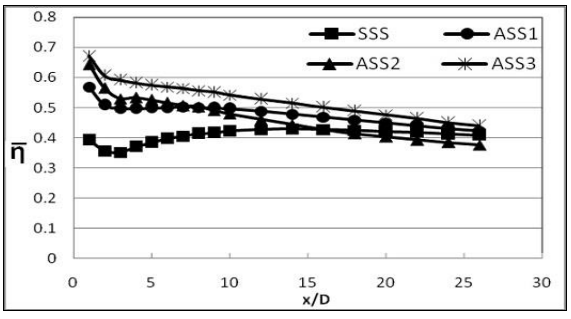

(b)VR = 1.0

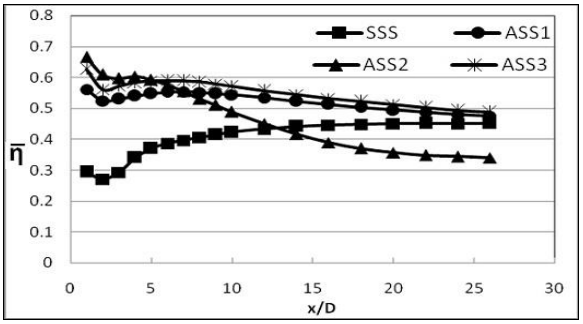

(c)VR = 2.0

Fig. 11 Spanwise-Averaged film cooling effectiveness of different models for ***staggered*** arrangement

For staggered arrangement, Fig. 10 shows that the highest film cooling effectiveness is given by model ASS3 along the test surface for all studied velocity ratios. At VR = 0.5, the adding of Anti-vortex holes slightly affects the film cooling effectiveness value due to lack of air flow. At high velocity ratios, the trend of anti-vortex models is changed as compared with SSS model.

3.3. Detailed film cooling effectiveness

The detailed film cooling effectiveness distributions of different models for in-line and staggered arrangements are shown in Figs. 11 and 12 respectively. For in-line arrangement, with model SSI, as the velocity ratio increases the film cooling effectiveness decreases. In anti-vortex cases, a part of the coolant flow is moving through the anti-vortex holes which help to increase the film cooling effectiveness along the areas between main holes. As the velocity ratio increases the film cooling effectiveness along the test surface appears to be close to each other for both ASI2 and ASI3 models. At VR = 0.5, Fig. 12 shows that the change of position of anti-vortex holes does not give a significant effect on the film cooling effectiveness. While at high velocity ratio (VR = 2), Model ASI3 gives the highest effectiveness as compared with other anti-vortex models.

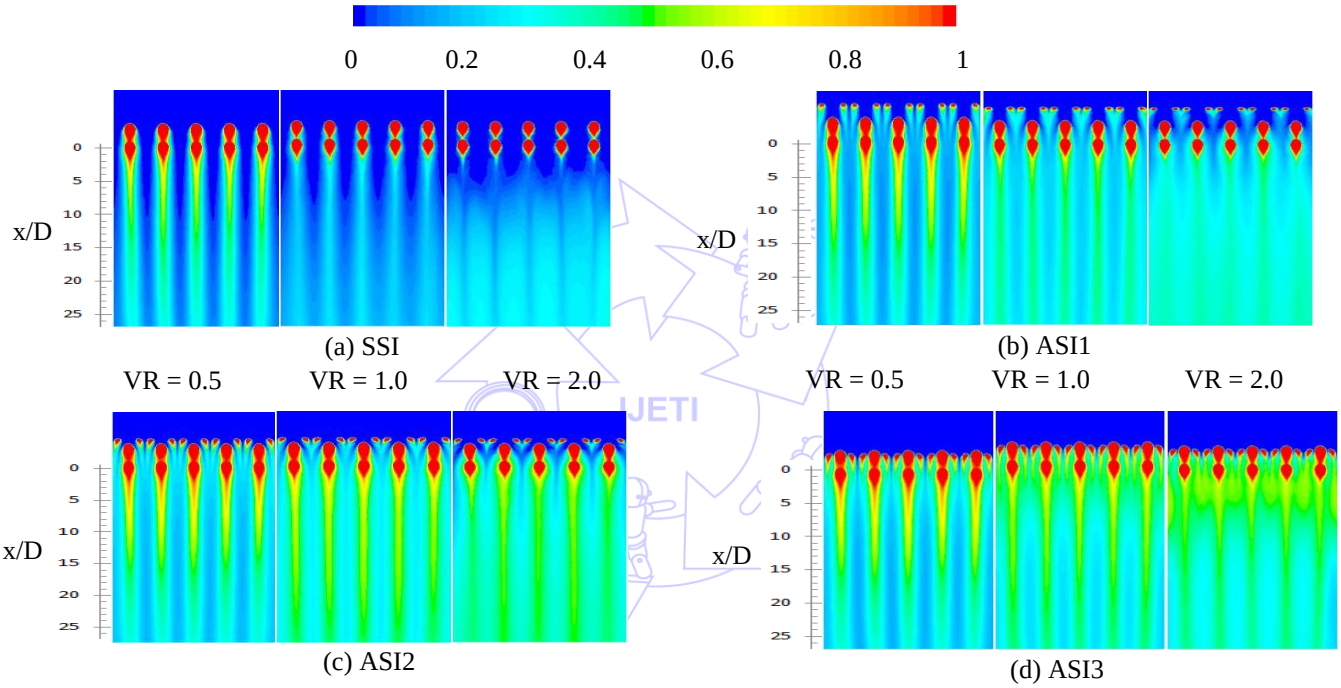

Fig. 12 Detailed film cooling effectiveness distributions of different models for in-line arrange at different velocity ratios

For staggered arrangement, the film cooling effectiveness for all studied cases is high as compared with in-line arrangement. Fig. 13 shows that the highest film cooling effectiveness is given by model ASS3 at all studied velocity ratios. The figure shows also that the coolant flow of the first row (downstream row) is attracted to the centerline. This is maybe due to a suction effect from the moving of the coolant flow from the second row (upstream row) which doesn't happen in in-line arrangement. The position of the anti-vortex holes gives a significant effect on the film cooling effectiveness. For model ASS1 the anti-vortex holes are coming out upstream far from the first and second rows of main holes; this gives a chance to the anti-vortex flow to move above both rows and try to damp them along the test surface. For that aspect, the film cooling effectiveness value downstream the second row is close to that downstream the first row. While for model ASS2, the anti-vortex holes are still upstream but close to the second row. This will cause a higher damping for the flow coming out from the second row. So the film cooling effectiveness downstream the first row holes will decrease rapidly along the test surface (Fig. 11). For model ASS3, the anti-vortex holes are in-line with the second row of main holes. Both anti-vortex holes and second row holes will try to damp the flow of the first row holes causing increasing of film cooling effectiveness downstream the first row holes.

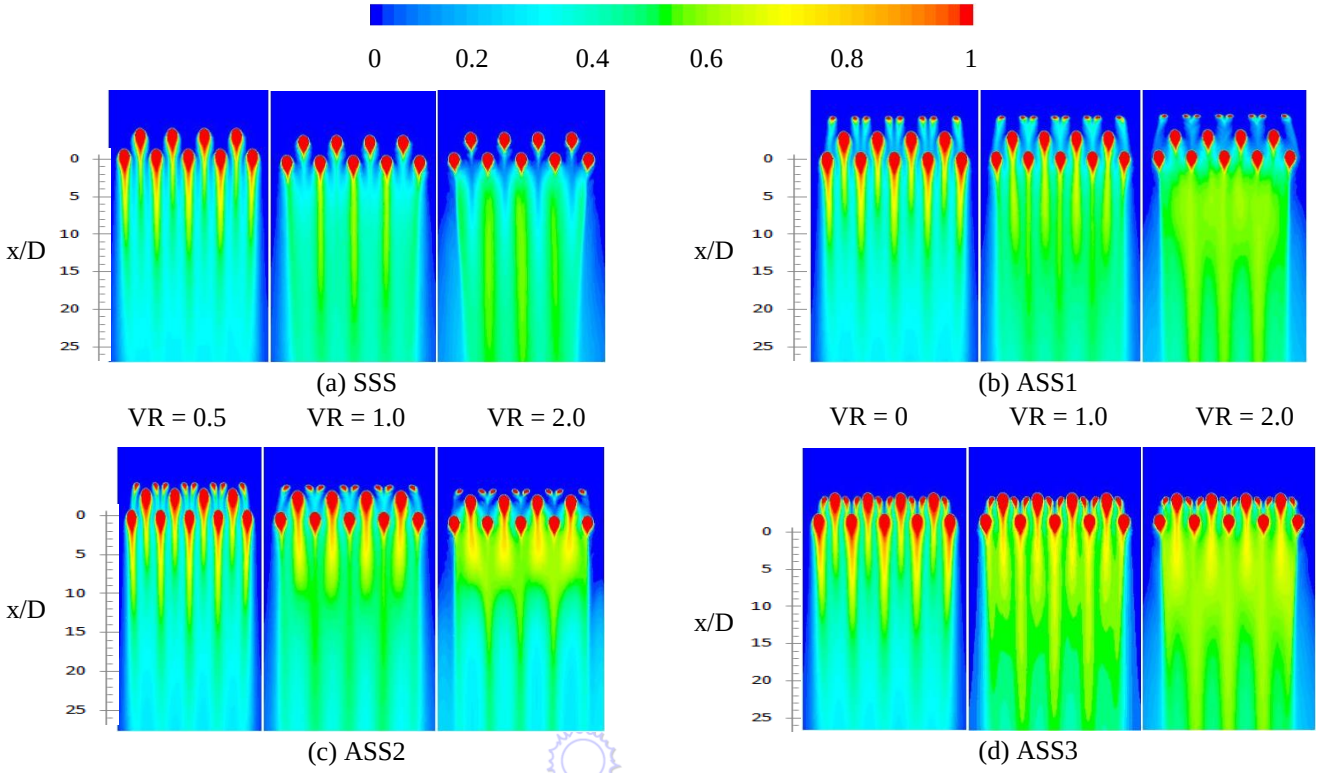

Fig. 13 Detailed film cooling effectiveness distributions of different model for ***staggered*** arrange at different velocity ratios

3.4. Overall averaged film cooling effectiveness

The overall area at which the averaged film cooling is calculated ranged from x/D =0 to x/D = 26, and z/D = -1.5 to z/D = 1.5 for y/D =0. Figs. 14 and 15 show the overall averaged film cooling effectiveness of different models with velocity ratio for in-line and staggered arrangements respectively. For in-line arrangement, Fig. 14 shows that the overall film cooling effectiveness decreases as the velocity ratio increases with SSI model due to higher momentum which allows the cooling jet to penetrate the mainstream flow. While, model ASI1 shows a constant overall effectiveness at different velocity ratio. With models ASI2 and ASI3, the overall effectiveness slightly increases as the velocity ratio increases because the addition of anti-vortex holes reduce the momentum of the main hole flow. The highest overall effectiveness occurs with model ASI3 due to the position of the anti-vortex holes.

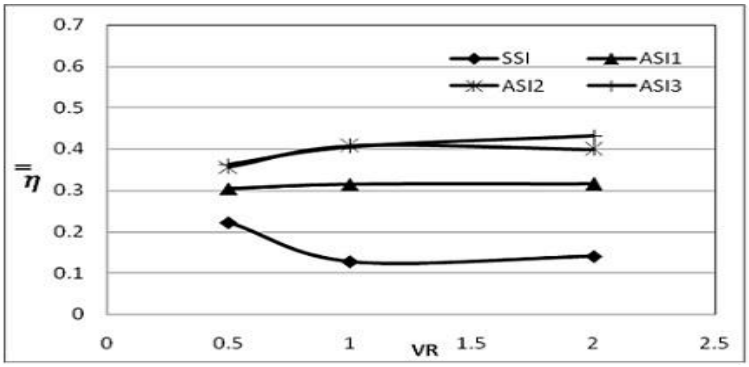

Fig. 14 The overall averaged film cooling effectiveness of different models for ***In-line*** Arrange with different velocity ratios

For staggered arrangement, Fig. 15 shows that the overall effectiveness remains constant as the velocity ratio increases with model SSS. While with studied anti-vortex models, as the velocity ratio increases the overall effectiveness increases because the position of anti-vortex holes helps in mitigating the flow coming out from the main holes and keep it moving beside the test surface. The Figure shows that the highest effectiveness is given by model ASS3 at all studied velocity ratios.

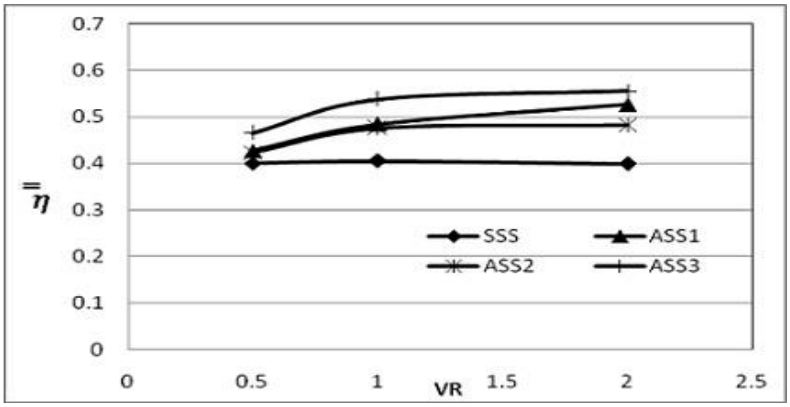

Fig. 15 The overall averaged film cooling effectiveness of different models for ***staggered*** Arrange with different velocity ratios

4. Conclusion

In the present study the adiabatic film cooling effectiveness on flat with two in-line and staggered rows of injection holes was investigated. The anti-vortex holes technique has been used to enhance the film cooling from two rows arrangements. Computational model for single row of circular film cooling holes and single row of circular film cooling holes supplemented with anti-vortex holes is validated well with an experimental works available in literature and showing good agreement with the experiments. The results show that

(1) The adiabatic film cooling effectiveness has been presented in details.

(2) The staggered arrangement provides much higher effectiveness than the in-line arrangement.

(3) The presence of anti-vortex holes provides higher effectiveness in both in-line and staggered arrangements.

(4) The presence of anti-vortex holes provides better cooling protection along the area between main holes.

(5) The position of anti-vortex holes has a significant effect with high velocity ratios.

(6) The film cooling effectiveness increases as the anti-vortex holes outlet is much closer to the second row of main holes.

References

[1] R. J. Goldstein, E. R. G. Eckert, V. L. Eriksen, and J. W. Ramsey, "Film cooling following injection through inclined circular tubes," Israel Journal of Technology, vol. 8, no. 1-2, pp. 145-154, 1970.

[2] J. Andreopoulous, and W. Rodi, "Experimental investigation of jets in crossflow journal of fluid mechanics," vol. 138, pp. 93-127, 1984.

[3] B. A. Haven, D. K. Yamagata, M. Kurosaka, S. Yamawaki, and T. Maya, "Anti-kidney pair of vortices in shaped holes and their influence on film cooling effectiveness," ASME Paper, no. 97-GT-45, pp. V003T09A007, 1997.

[4] C. A. Lemmon, A. Kohli, and K. A. Thole, "Formation of counter-rotating vortices in film-cooling flows," ASME Paper, no. 99-GT-161, 1999.

[5] S. Dhungel, A. Phillips, S. V. Ekkad, and J. D. Heidmann, "Experimental investigation of a novel anti-vortex film cooling hole design," ASME Paper, no. GT2007-27419, 2007.

[6] J. D. Heidmann, "A numerical study of anti-vortex film cooling designs at high blowing ratio," NASA/TM—2008-215209, 2008.

[7] J. D. Heidmann, S. Ekkad, "A novel antivortex turbine film-cooling hole concept," Journal of Turbomachinery, ASME, vol. 130, July 2008.

[8] A. H. Mostafa, T. Mikhael, S. S. Ayad, and K.M. El-Shazly, "An investigation of the effect of anti-vortex film cooling on flat plate," Tenth International Congress of Fluid Dynamics (ICFD 10), AinSoukhna, Red Sea, Egypt, pp. 16-19 December, 2010.

[9] P. M. Ligrani, J. M. Wigle, S. Ciriello, S. W. Jackson, "Film-cooling from holes with compound angle orientations: part 1 – results downstream of two staggered rows of holes with 3d spanwise spacing," ASME J. Heat Transfer, vol. 116, pp. 341-352, May 1994.

[10] C. H. N. Yuen, R. F. Martinez-Botas, "Film cooling characteristics of rows of round holes at various streamwise angles in a crossflow: part I. Effectiveness," Int J Heat Mass Transfer, vol. 48, pp. 4995-5016, 2005.

[11] J. F. Muska, R. W. Fish, M. Suo, "The additive nature of film cooling from rows of holes," ASME J. Eng. Power, vol. 98, no. 4, pp. 457- 464, 1976.

[12] W. O. Afejuku, N. Hay, D. Lampard, "Measured coolant distributions downstream of single and double rows of film cooling holes," ASME J. Eng. Power, vol. 105, no. 1, pp. 172-177, 1983.

[13] B. A. Jubran, B. Y. Maiteh, "Film cooling and heat transfer from a combination of two rows of simple and/or compound angle holes in in-line and/or staggered configuration," Heat and Mass Transfer, vol. 34, pp. 495-502, 1999.

[14] J. Ahn, I. S. Jung, J. S. Lee, "Film cooling from two rows of holes with opposite orientation angles: injectant behavior and adiabatic film cooling effectiveness," International Journal of Heat and Fluid Flow, vol. 24, pp. 91-99, 2003.

[15] F.H. Asghar, M.J. Hyder, "Computational study of film cooling from single and two staggered rows of novel semi-circular cooling holes including coolant plenum," Energy Conversion and Management, vol. 52, pp. 329-334, Jan. 2011.

[16] T. I. P. Shih, Y.L. Lin, M. K. Chyu, and S. Gogineni, "Computations of film cooling from Holes with Struts," ASME Paper No. 99-GT-282, 1999.

[17] S. Kapadia, S. Roy, and J. Heidmann, "Detached eddy simulation of turbine blade cooling," AIAA-2003-3632, 36th Thermophysics Conference, Orlando, Florida, June 2003.

[18] B. Johnson, K. Zhang, W. Tian, and H. Hu, "An experimental study of film cooling effectiveness by using PIV and PSP techniques", AIAA 2013-0603, 51st AIAA Aerospace Sciences Meeting including the New Horizons Forum and Aerospace Exposition, Grapevine (Dallas/Ft. Worth Region), Texas, pp. 07-10 January 2013.

Nomenclature

D	Film cooling main hole diameter (m)	T_f	Local film temperature (K)
d	Film cooling anti-vortex hole diameter (m)	T_m	Mainstream air temperature (K)
VR	Velocity Ratio = U_c/U_m	U_c	Coolant air velocity (m/s)
BR	Blowing Ratio =$(\rho_c U_c/\rho_m U_m)$	U_m	Mainstream air velocity (m/s)
MR	Momentum Ratio = $(\rho_c U_c^2/\rho_m U_m^2)$	x	Distance from the upstream row centerline (m)
Re_x	Free stream Reynolds number = U_m*x/ν_m	ν	Kinematic viscosity of the fluid (m^2/s)
Re_D	Injectant Reynolds number = U_c*D/ν_c	$\bar{\eta}$	Average film cooling effectiveness
T_{aw}	Adiabatic wall temperature (K)	$\bar{\bar{\eta}}$	Overall film cooling effectiveness
T_c	Coolant air temperature (K)		